Ocean Modelling 193 (2025) 102456

Contents lists available at ScienceDirect

Ocean Modelling

journal homepage: www.elsevier.com/locate/ocemod

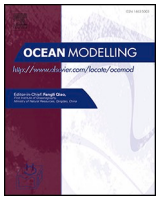

Upgrade of the Chilean Wave Atlas database

Sebastian Omar Correa Araya [a,*], Catalina Aguirre [b], Diego Becerra [c], Mauricio Molina [d], Pablo Vilchez [d], Sergio Bahamóndez [e]

[a] School of Oceanic Engineering, Universidad de Valparaíso, Valparaíso, Chile
[b] School of Ocean Engineering, Universidad de Valparaíso,Valparaíso, Chile.Center for Climate and Resilience Research (CR)2, Chile (FONDAP/ANID 1523A0002)
[c] ECOTECNOS S.A., Valparaíso, Chile
[d] School of Ocean Engineering, Universidad de Valparaíso, Valparaíso, Chile
[e] School of Ocean Engineering, Universidad de Valparaíso, Valparaíso, Chile. Department of Geophysics, Universidad de Concepción, Concepción, Chile

ARTICLE INFO

Keywords:
Wave hindcast
Calibration and validation
Satellite significant wave height
Wave buoys observations
Chile
WAVEWATCH III

ABSTRACT

The Chilean Wave Atlas (AOC1), a reliable hindcast developed in 2017 for the academic and engineering community, diminished its usefulness due to the obsolescence of wind data provided by ERA-Interim reanalysis. This study presents the calibration and validation of a new wave hindcast forced using hourly winds data from ERA5 reanalysis. A total of 24 simulations were conducted: 15 using the semi-empirical ST4 parameterization and 9 using the observed-based ST6 parameterization, both implemented in WaveWatch III. Model results were compared with in-situ wave data from buoys along the Chilean coast. Generally, the ST4 physics package demonstrated superior performance with minimal variability in error statistical parameters between simulations. However, the observed-based ST6 parameterization produced the best results for simulating wave direction. By defining a multi-criteria performance score, the optimal model configuration was selected, and a new hindcast was generated for the period between 1979 and 2022. This hindcast includes hourly fields of significant wave height, mean and peak wave period, and mean and peak wave direction for the Pacific Ocean, as well as 72 locations with directional spectra. The upgraded Chilean Wave Atlas (AOC3) significantly improves the performance of AOC1 when compared with satellite-derived wave heights along the Chilean coast. Furthermore, the AOC3 data show good performance compared to other freely available hindcasts.

1. Introduction

Wind-driven waves depend on wind speed and direction. Specifically, the amount of time the wind blows over the ocean surface and the distance that the wind blows in a particular direction over an area of influence, which is referred to as the fetch. The waves in this area are called wind sea and are characterized by waves that are shorter in wavelength and higher in frequency. Once energy balance is achieved and/or when the wave propagation speed is higher than the wind speed, waves stop growing and can propagate across an ocean basin as wave called swell, playing a relevant role in several processes at the air-sea interface, which affect both the atmospheric and oceanic mixing layers e.g. (Cavaleri et al., 2012; Babanin, 2017).

When waves propagate towards the coast, they transition from deep waters, where there is no interaction between waves and the seabed, to intermediate and shallow waters, where the reduction in depth allows waves to be affected by the seabed, which significantly changes the characteristics of the waves such as steepness and propagation direction, among others. Waves generate coastal currents, erosion and accretion along the shoreline (Komar, 1998), and in marginal ice zones, feedback processes with marine ice can play a relevant role in coastal morphology (Kousal et al., 2022). Moreover, extreme wave events can cause overtopping, displacement of coastal protection elements, or even destruction of coastal structures such as breakwaters, piers, ports, and harbors (Goda, 2010). Thus, characterizing wave climate is an essential task not only for advanced scientific knowledge but also for the development of oceanic and coastal infrastructure. To properly characterize the wave climate, it is necessary to have data spanning at least a couple of decades (Liu & Frigaard, 1999). In particular, in Chile, the wave climate must be characterized using a database with a temporal extension of at least 20 years to obtain the required construction permits along the shoreline, which the Hydrographic and Oceanographic Service of the Chilean Navy grants (SHOA, 2009).

Measuring the different wave parameters includes methods such as

* Corresponding author.
E-mail address: sebastian.correa@uv.cl (S.O.C. Araya).

https://doi.org/10.1016/j.ocemod.2024.102456
Received 24 June 2024; Received in revised form 9 October 2024; Accepted 21 October 2024
Available online 19 November 2024

visual observations recorded by ship captains, directional wave buoys, submerged acoustic or pressure sensors, high-frequency radars, and remote methods such as satellite altimetry (e.g. Silva, 2005). Data gathering through direct observation is costly. Moreover, in situ methods only allow the characterization of the waves in limited areas and for a short period, while satellite observations have temporal and spatial limitations. Thus, numerical wave modeling has emerged as a way to bridge the gap between these limitations, achieving reasonable simulated approximations of observed waves in a shorter period with fewer resources. These modeling can be oriented towards a historical reconstruction of the waves (hindcasting), obtaining good levels of performance (e.g. J. Liu et al., 2022; Soran et al., 2022; Smith et al., 2021; Liu et al., 2021; Amarouche et al., 2019; Shimura & Mori, 2019; Beyá et al., 2017), as well as short-term wave forecasting from 7 up to 16 days (e.g. Cao et al., 2007; https://marejadas.uv.cl), and also long-term projections of wave climate under different anthropogenic climate change scenarios (Pavlova et al., 2022; Badriana & Lee, 2020; Hemer et al., 2013; Fan et al., 2012).

Several efforts have been made to characterize the wave climate in Chile. Aguirre et al., (2017) present wave climatology in the Southeast Pacific separating the swell and sea components that show the main contribution of the Southern Ocean swell to wave climate in this region. More regionally, Mediavilla & Sepúlveda (2016) carried out a study characterizing wave energy for central Chile. In 2016, the first Chilean Wave Atlas (Atlas de Oleaje de Chile, https://oleaje.uv.cl/) was developed using the WaveWatch III model calibrated and validated with in-situ and remote wave observations (Beyá et al., 2016; Beyá et al., 2017). The generated wave database (hindcast), called AOC1 due to its initials in Spanish, was forced with surface winds from the ERA-Interim reanalysis. However, ERA-Interim was discontinued in 2019 and replaced by ERA5, so AOC1 cannot be extended beyond 2019. This work presents an update of the Chilean Wave Atlas with a new database generated using the WaveWatch III 6.07 model forced with ERA5 using hourly wind fields 10 m above the sea surface, including over-sea ice coverage. The temporal resolution of the inputs and outputs of the model was increased, achieving a calibrated and validated wave hindcast for the coasts of Chile from 1979 to 2023, which can be extended in the future. Maintaining a validated wave model is crucial in vast coastal regions of Chile where observed data is scarce, and the lack of long-term reliable measurements poses a significant challenge to understanding local wave climate and variability. The document's structure is as follows: section 2 briefly describes the model used, the initial configuration for each simulation, the procedure to select the best performance, and details of available data for calibration and validation. Section 3 describes the results of the calibration carried out using buoy data and the validation using data from other hindcasts and satellite altimetry. Section 4 discusses the principal results and their scope, and the conclusions of this work are finally presented in section 5.

2. Materials and methods

2.1. Spectral wave model

The third-generation wave model Wavewatch III (WW3) version 6.07 was used to run the simulations (WW3DG, 2019). This numerical model is widely used by the most prestigious institutions in the world and is continuously improving the representation of the physical processes involved in this phenomenon. WW3 is a wave spectral model using an Eulerian approach to simulate wind-generated wave energy. To estimate the evolution of wave energy in space and time, the model uses the finite difference technique to resolve the Spectral Action Balance Equation.

$$\frac{\partial N(k,\theta,X,t)}{\partial t}+\nabla_X\left(C_g+U\right)N(k,\theta,X,t)+\frac{\partial}{\partial k}\dot{k}N(k,\theta,X,t)+\frac{\partial}{\partial\theta}\dot{\vartheta}N(k,\theta,X,t)=\frac{S_t(k,\theta,X,t)}{f} \quad (1)$$

To compile WW3, specific physical and computational parameters within the switch file must be activated and deactivated. In this research, the main parameterizations used are presented in Table 1.

2.2. Model configuration

To force the model, we used data generated by the European Center for Medium-Range Weather Forecast (ECMWF) in its most recent reanalysis ERA5 (Hersbach et al., 2020). Specifically, the hourly U and V components of the wind at 10 m above the surface and sea ice concentration, with a spatial resolution of 0.25°x0.25° ERA5 is a database that offers the best performance for surface wind speed and variability compared to other reanalyses (Ramon et al., 2019).

The digital elevation model ETOPO2v2 was used for bathymetry representation, which has a 2-minute spatial resolution (NOAA National Geophysical Data Center, 2006). The coastline database used was the Global Self-consistent Hierarchical High-resolution Shoreline (GSHHS) developed by Wessel & Smith (1996 &2015) with a spatial resolution of 5 [km]. A 1°x1° bathymetric grid was created using the GRIDGEN software (Chawla & Tolman, 2007). A spectral discretization with the frequency increment factor 1.1, the initial frequency 0.035 Hz, 29 frequencies, and 24 directions was used. The maximum global time step was 900 s. The numerical domain covered the entire Pacific Ocean with a regular 1°x1° grid, extending from longitude 100°W to 299°W and latitude 80°N to 70°S (Fig. 1), with a total of 200 × 151 calculation nodes. As no boundary conditions are applied, the model performs well in the interior region of the domain. The exact longitudes and latitudes of these well-performing region are indicated in Fig. 1.

The outputs of the numerical model have been obtained with an hourly temporal resolution, which include the following wave parameters: significant wave height (Hs), mean wave direction (Dm), peak wave direction (Dp), peak wave frequency (fp), mean wave period (Tm) and the directional spectra of wave energy at 72 nodes located every 1° of latitude off the coast of Chile and island areas, and other points on the eastern edge of the Pacific Ocean, whose locations are presented in Fig. 1.

2.3. Wave hindcast calibration

The ST4 and ST6 switches were used to calibrate the model. In the case of ST4, the methodology proposed by Ardhuin et al. (2010) was used. This method consists of modifying the coefficients involved in the formulation of growth (*Sin*) and dissipation (Sds) of wave energy due to the effects of surface wind (Table 3). Particularly, βmax is the maximum

Table 1
Switch parameters used (modified parameters in bold).

Parameter	Description	Switch
Propagation schemes	Higher-order schemes	PR3
	Third-order propagation scheme	UQ
Flux Computation	Flux computation included in source terms	FLX0
Linear input	Spectral seeding	SEED
Inputs and dissipation	ST4 Ardhuin et al. (2010) source term package	ST4
	ST6 BYDRZ source term package	ST6
	No stability correction	STAB0
Nonlinear interactions	Discrete interaction approximation (DIA)	NL1
Botton friction	SHOWEX bottom friction formulation	BT4
Depth-induced breaking	Battjes-Janssen	DB1
Miscellaneous switches	Use Miche-style shallow water limiter	MLIM
	Correct wind speed for current velocity.	RWND

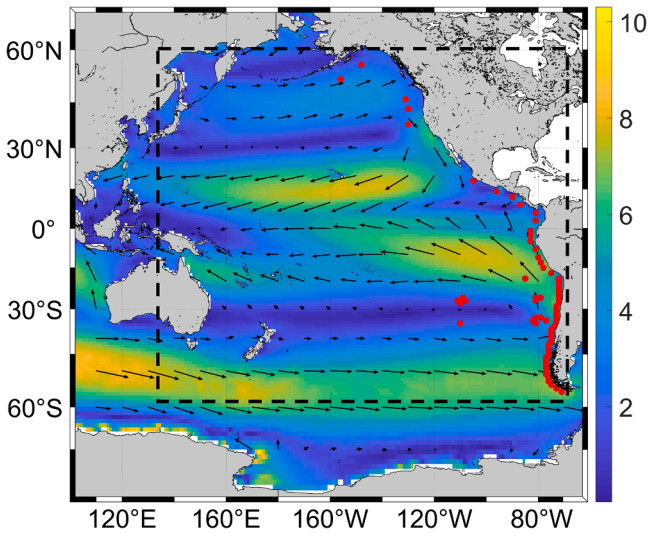

Fig. 1. Mean wind speed at 10 m above the surface in m/s and direction ° (black arrows) in the period 1979–2022. Red dots indicate the locations of spectral wave data outputs. The segmented black line indicate well performs region (i.e. Where the simulated Hs BIAS is <10 % compared with satellite Hs).

value of wind-wave coupling in full wind input source term, Cds is a non-dimensional constant in the swell dissipation equation, and Br is the threshold for the saturation spectrum that determines the dissipation of energy associated with wave breaking. On the other hand, the ST6 package is an observation-based parametrization approach (Rogers et al., 2012; Zieger et al., 2015). Here, nine simulations use the ST6 package but with different coefficients a_0 and b_1 values, which control the effect of opposing wind and swell energy dissipation, respectively (Table 4). Following the methodology used by Beyá et al. (2017), the model is compared with buoy records using various statistical error parameters, which are combined to calculate a "Global Model Performance Score" (MPS), which ranges from 0 to 1, with values closer to 1 indicating better performance.

$$MPS^{EP}_{(i,k,l)} = \sum_{j=1}^{4} \omega^{EP}_{(j)} \times \widehat{X}_{(i,j,k,l)} \; for \;\; j = MAE,\; R^2, RMSE,\; BIAS \tag{2}$$

Where i represents the index of each test, j is the index of the error parameter, k is the index of the wave statistical parameter and l is the index type of data, $\omega^{EP}_{(j)}$ is the weight factor, MAE is mean absolute error, R^2 coefficient of determination, RMSE root mean square error and BIAS tendency of a statistic. Table 2 presents the formulations of these error metrics where N is the length of data, P_i predicted data, O_i observed data. Since these error metrics span different ranges, a normalization process is applied to scale their values between 0 and 1. Finally, the simulation with the highest MPS, considering the 15 calibrations of ST4 and 9 of ST6 (24 cases), was used to generate the AOC3 wave hindcast between 1979 and 2023.

It is worth noting that because of the cyclic nature of the wave direction, some caution must be taken when calculating the error metrics. However, in our study area, wave directions span a limited range of directions (200° to 300°) at all buoy locations (not shown). Hence, in this case, the formulas of error metrics are also valid for both wave directions parameters Dm and Dp.

Table 2
Error statistics and normalization.

Error statistics	Normalization
$BIAS = \frac{1}{N}\sum_{i=1}^{N} P_i - O_i$ (3)	$\hat{x} = \frac{\lvert x\rvert - \min(\lvert x\rvert)}{\max(\lvert x\rvert) - \min(\lvert x\rvert)}$ for BIAS
$MAE = \frac{1}{N}\sum_{i=1}^{N} \lvert P_i - O_i\rvert$ (4)	$\hat{x} = 1 - \frac{x - \min(x)}{\max(x) - \min(x)}$ for $x = MAE, RMSE$
$RMSE = \sqrt{\frac{1}{N}\sum_{i=1}^{N} (P_i - O_i)^2}$ (5)	$\hat{x} = \frac{x - \min(x)}{\max(x) - \min(x)}$ for $x = R^2$
$R^2 = \frac{\left(\sum_{i=1}^{n}(O_i - \overline{O})(P_i - \overline{P})\right)^2}{\left(\sum_{i=1}^{n}(O_i - \overline{O})^2\right)\left(\sum_{i=1}^{n}(P_i - \overline{P})^2\right)}$ (6)	

Table 3
Scenarios for source terms parameters **ST4**[11].

	ST4 scenarios $Bmax$	Growth S_{in} C_{ds}	Dissipation S_{ds} B_r
C.1	1.52	-2.2×10^{-5}	9×10^{-4}
C.2	1.58	-2.2×10^{-5}	9×10^{-4}
C.3	1.62	-2.2×10^{-5}	9×10^{-4}
C.4	1.65	-2.2×10^{-5}	9×10^{-4}
C.5	1.70	-2.2×10^{-5}	9×10^{-4}
C.6	1.52	-3.0×10^{-5}	9×10^{-4}
C.7	1.52	-2.2×10^{-5}	8×10^{-4}
C.8	1.58	-3.0×10^{-5}	9×10^{-4}
C.9	1.58	-2.2×10^{-5}	8×10^{-4}
C.10	1.62	-3.0×10^{-5}	9×10^{-4}
C.11	1.62	-2.2×10^{-5}	8×10^{-4}
C.12	1.65	-3.0×10^{-5}	9×10^{-4}
C.13	1.65	-2.2×10^{-5}	8×10^{-4}
C.14	1.70	-3.0×10^{-5}	9×10^{-4}
C.15	1.70	-2.2×10^{-5}	8×10^{-4}

Table 4
Scenarios for source terms parameters ST6.

ST6 scenarios	Growth S_{in} a_0	Dissipation S_{swd} b_1
C.16	0.09	4.1 × 10–3
C.17	0.04	2.5 × 10–4
C.18	0.04	3.2 × 10–3
C.19	0.04	4.1 × 10–3
C.20	0.09	2.5 × 10–4
C.21	0.09	3.2 × 10–3
C.22	0.14	2.5 × 10–4
C.23	0.14	3.2 × 10–3
C.24	0.14	4.1 × 10–3

2.4. Data used for model calibration and validation

Wave data measured with buoys belonging to the Hydrographic and Oceanographic Service of the Chilean Navy (SHOA) were used to calibrate the model. The geographical locations of the instruments and measurement periods are indicated in Table 5 and Fig. 2.

Different wave hindcasts that are available were used to validate the AOC3 database (Table 6). Wave data from different ECMWF products are considered, such as ERA-Interim, which is a reanalysis from 1979 to August 2019 (Dee et al., 2011) and ERA5, which corresponds to the fifth-generation global reanalysis successor to ERA-Interim, whose temporal extension is from 1940 to the present (Hersbach et al., 2020). In addition, a database is used from the Collaboration for Australian Weather and Climate Research (CAWCR), which is between the Commonwealth Scientific and Industrial Research Organization (CSIRO) and the Australian Bureau of Meteorology. This is a hindcast of forced waves with winds from the NCEP CFSR reanalysis (1979–2010) and NCEP CFSv2 (2011–2013)(Durrant et al., 2013). The WW3-ST6-CONV data, which is a hindcast of waves forced with the ERA5 conventional surface winds (U_{10}) between 1979 and 2019 using the ST6 physical parameterizations, is also used (Liu et al., 2021). The Chilean Wave Atlas AOC1 described in Beyá et al. (2017), is also compared with the new database-generated AOC3. Table 6 details each wave database's forcings and spatial and temporal resolution. The lowest temporal resolution of 6 h is presented in the ERA-Interim hindcast, so all databases were

Table 5
Location of the buoys for calibration from north to south. .[21]

Location	Latitude	Longitude	Start date	End date	# data
Iquique	20°14.9′S	70°14,8′W	13–09–2018	31–12–2020	5592
Valparaíso	32°59.7′S	71°49.5′W	01–08–2000	31–12–2019	15,690
Punta Curaumilla	33°08′S	71°49′W	16–06–2011	21–12–2013	6919
Lebu	37°35′S	73°45′W	16–09–2011	16–05–2012	2682
Corral	39°33′S	73°24′W	21–11–2012	30–07–2013	2068

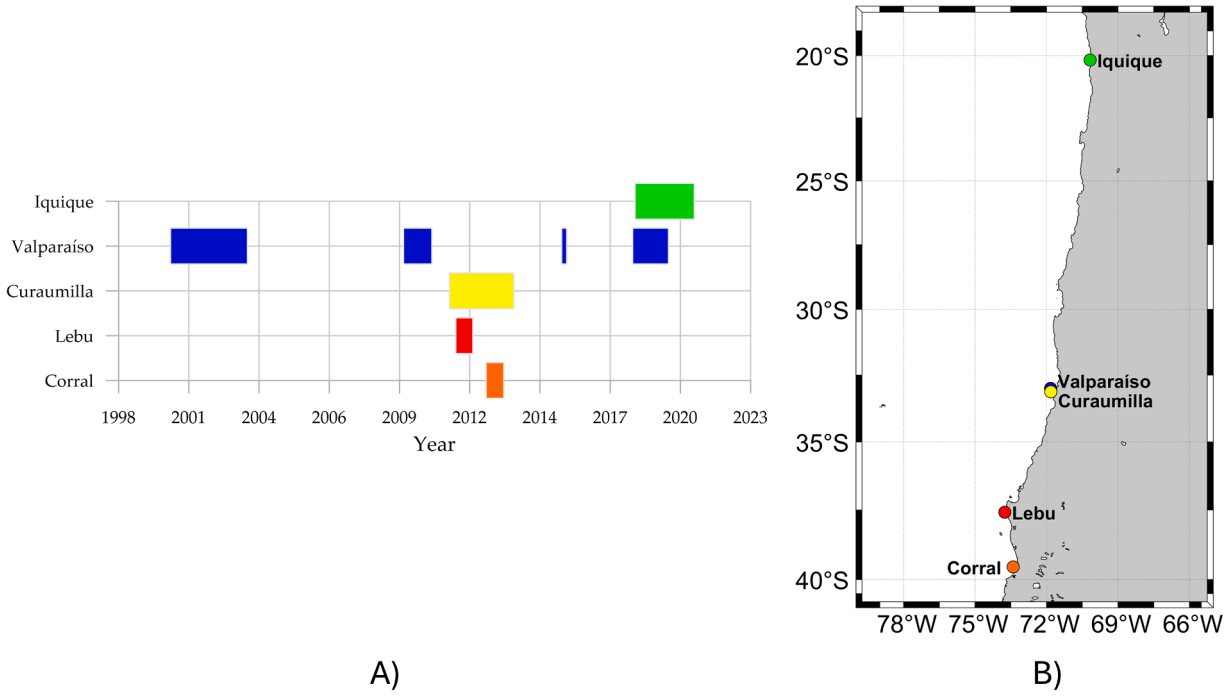

Fig. 2. Location of buoys. (left) Temporal extension of wave buoy measurements. (right) Location of wave buoy measurements.

Table 6
Details of hindcasts used.

Data Base	Wind input	Spatial resolution	Temporal resolution [Hrs]	Temporal extension
ERA-Interim	ERA-Interim	110 [Km]	6	1979–2019
ERA5	ERA5	0.5 °	1	1940-present
CAWR-CSIRO	CFSR	0.4°	1	1979–2010
WW3-ST6-CONV	ERA5	0.25°	3	1979–2019
AOC1	ERA-Interim	1°	3	1979–2015

evaluated at this resolution for the analyses. All data was extracted at the nearest grid point to the Valparaíso buoy.

In addition to the buoy and hindcast data available, satellite altimetry data corresponding to 10 missions carried out from 1991 to 2018 were used for validation. This database was obtained from the Sea State CCI dataset v1 is freely available on the ESA CCI website (https://data.ceda.ac.uk/neodc/esacci/sea_state/data, last access: 7 November 2022) at http://anon-ftp.ceda.ac.uk/neodc/esacci/sea_state/data/v1.1_release/ (last access:7 November 2022) (Dodet et al., 2020), and the characteristics of the altimetry sensors are detailed in Table 7.

The satellite significant wave height (HS_{SAT}) along-track L2P is used from latitude 15°S to 75°S and longitude 120 °W to 65°W, an extension that covers most of the Chilean Maritime Zone, including territorial seas along the mainland and surrounding islands (Fig. 3). For each location of the model's spectral outputs, HS_{SAT} was extracted for a surrounding area of 0.5°x0.5°, and an hourly average was performed to compare it with the outputs of the wave model (Fig. 3).

3. Results

3.1. Wave model calibration

Time series of the wave parameters simulated using different parameterizations were compared with wave observations recorded by a buoy located off the coast of Valparaíso (Fig. 4). One week from July 9 to 15, 2019, was selected, during which the buoy registered an extreme wave event. During this event, the maximum Hs reached 3.5 m, corresponding to the 95th percentile of the data measured during that campaign. The simulated Hs agrees with observations with slight variation throughout the different simulations when using the ST4 package, while more variability is found between simulations using ST6 parametrization (Fig. 4a). Overall, the variability of the Tm records is well-represented by the model. However, the values are slightly overestimated, and the increase in Tm associated with the extreme wave event begins approximately one day earlier than was observed. In ST4, the Tm exhibits maximum variations between simulations when wave intensity increases, while the differences become negligible once the peak of the extreme event is reached. In contrast, the opposite occurs in the ST6 simulations; they exhibit less variability in Tm during high wave energy and more variation in calmer conditions (Fig. 4b). The model has more difficulty reproducing the variability of the peak period ($Tp = fp^{-1}$); all simulations indicate that sudden Tp changes are time-lagged and

Table 7
Satellite missions used for validation (Dodet et al., 2020).

Mission	Instrument	Band	Covered period	Repeat period (days)	Altitude (km)	Inclination (°)	Source product
ERS-1	RA	Ku	1991–2000	35	785	98.52	OPR [ESA/FPAF]
TOPEX	NRA	Ku	1992–2006	10	1336	66	MGDR [CNES]
ERS-2	RA	Ku	1995–2011	35	785	98.52	OPR [ESA/FPAF]
GFO	GFO-RA	Ku	1998–2008	17	800	108	GDR/POE [NOAA]
JASON-1	Poseidon-2	Ku	2001–2013	10	1339	66	GDR vE [AVISO]
EVISAT	RA-2	Ku	2002–2012	35	799	98.55	GDR v2.1 [ESA/F-PAC]
JASON-2	Poseidon-3	Ku	2008–2019	10	1336	66	GDR vD [AVISO]
CRYOSAT-2	SIRAL	Ku	2010-Ongoing	369	717	92	IGDR [NOAA]
SARAL	AltiKa	Ku	2013-Ongoing	35	785	98.55	GDR [AVISO]
JASON-3	Poseidon-3B	Ku	2016-Ongoing	10	1339	66	GDR vD [AVISO]

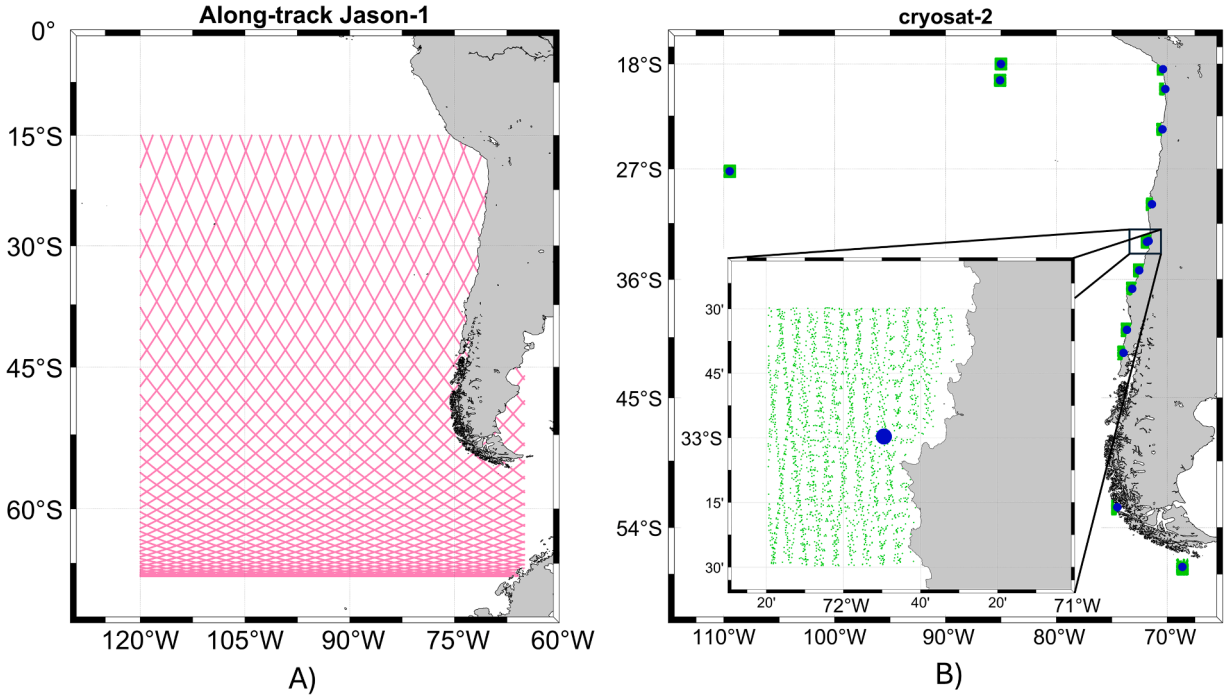

Fig. 3. Satellite along-track data. (left) Example of latitude and longitude filter application for Jason-1. (right) Example of cryostat-2 data (green dots) extraction close to the model spectral outputs (blue dots).

overestimated (Fig. 4c). Wave Dm exhibits a good fit to the observed data, except on July 9th, when the buoy records indicate a sudden change in Dm with eastward wave propagation, which the model fails to reproduce (Fig. 4d). Dm generally shows very low variability between simulations in the ST4 package, but higher variation is observed in ST6 simulations, particularly when the wave energy is increasing. Modeled Dp shows more variability between simulations than Dm, particularly in ST6 parametrization during the beginning of the extreme event. Furthermore, the arrival of the event occurred earlier in the model than the observed data, as shown in Dp times series lag (Fig. 4e).

To analyze the impact of different model parameterizations on the performance in representing wave parameters, Fig. 5 presents the MPS as a function of different coefficients used. The representation of Hs shows the best and most consistent performance in simulations using the ST4 package, as all MPS values are higher than 0.8, while the ST6 package only reaches similar MPS values at a couple of simulations (a_o=0.09; b_1=3.2 × 10^{-3} and a_o=0.14; b_1=2.5 × 10^{-4}). The best performance of Hs in ST4 parametrization is using a Cds=−3.0 × 10^{-5} with slightly higher values observed when βmax is between 1.58 and 1.65. In general, simulations using Cds = −2.2 × 10^{-5} present slightly lower MPS values in Hs. Specifically, with Cds = −2.2 × 10^{-5} and Br = 9 × 10^{-4}, an inverse relationship is observed between βmax and MPS, with model performance decreasing as βmax increases. Conversely, with Br = 8 × 10^{-4}, a direct relationship is observed between βmax and MPS, with model performance improving as βmax increases (Fig. 5a-d). Tm shows that ST4 and ST6 can reach similar model performance with MPS values close to 0.8 (Figure b-e). ST4 simulations consistently present higher MPS when Cds = −2.2 × 10^{-5} and Br = 9 × 10^{-4}, exhibiting also an increase with higher βmax. The best performance on Tm is found in an ST6 simulation when a_o=0.04 and b1=3.2 × 10^{-3} are used. However, the worst results are also observed in this package as the MPS strongly decreases when a higher a_o is used. Dm exhibits systematically better performance using the ST6 package than ST4. The best representation of Dm is observed with ao=0.09 independently of the b1 used. In ST4 simulations, no significant differences are observed in the MPS throughout the simulations. Tp shows better model performance in the ST4 package, particularly when using Br = 8 × 10^{-4} (Fig. 5c-F). However, the MPS for Tp significantly decreases when Cds = −2.2 × 10^{-5} and Br = 9 × 10^{-4}. In ST6 simulations, higher model performance is observed when a_o=0.14 and b_1=4.1 × 10^{-3}. In general, the simulated Dp performs better in ST4 than ST6, except when a_0=0,04 is used, and higher MPS are reached at a_0=0.14. In ST4 simulations, Dp shows worse when Cds = −2.2 × 10^{-5} and Br = 9 × 10^{-4}. Additionally, we show in the supplementary material the error metrics separately for each simulation in Figures S1 and S2 and separately for each buoy in Tables S1 to S5.

To visualize the behavior of the different statistical error metrics

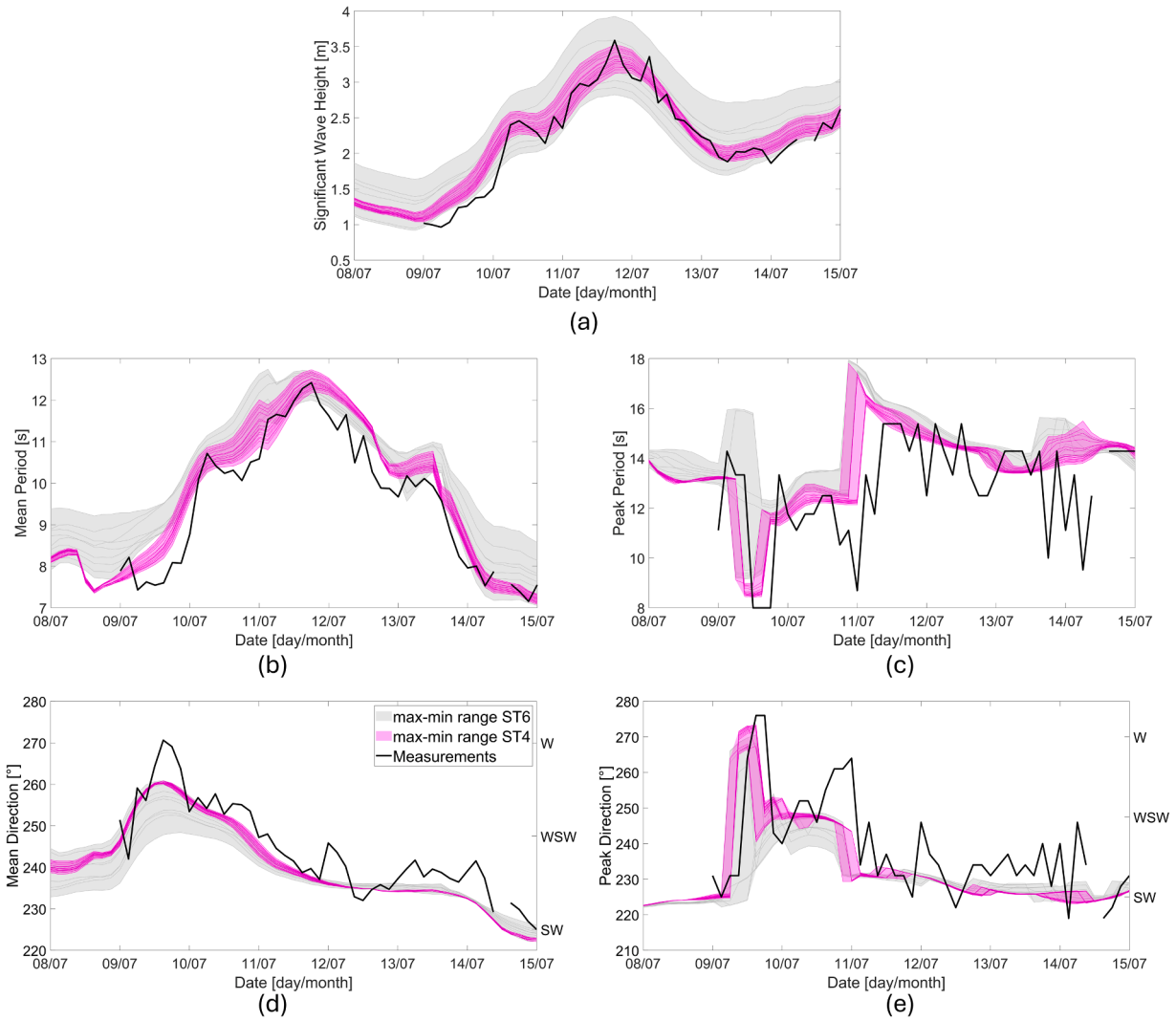

Fig. 4. Time series of wave parameters during an extreme event recorded by the wave buoy off Valparaiso(black), range of all **ST4** results (pink), and range of all **ST6** result (grey) for (a) Significant wave height (b) Mean period (c) Peak period (d) Mean direction and (e) Peak direction.

used in each of the calibrations—namely BIAS, root mean square error (RMSE), and Correlation Coefficient (R) diagrams were constructed using 19,595 simulation/observation data pairs (Fig. 6). Supplementary tables S1 to S5 present the error metrics for each buoy location in wave parameters with data availability. Hs shows similar correlation and error values in all the simulations conducted with the ST4 parameterization, with R close to 0.92 and RMSE approximately 0.33 m. The BIAS presents positive and negative values (±0.15 m), indicating either an overestimation or underestimation of Hs depending on the coefficients chosen in ST4. The simulations using the ST6 parameterization present slightly lower correlation values and higher error, values of $R = 0.90$ and RMSE = 0.35 m (Fig. 6a). Tm can be well represented with the ST4 and ST6 parameterizations, but results depend on the coefficients chosen. The best simulation shows R close to 0.85, RMSE of around 0.9 s, and an underestimation of Tm in 0.5 s. Lower skill variation among the different simulations is observed in the ST4 package (Fig. 6b). As evident in Fig. 4, the model's performance decreases for Tp, with the RMSE for Tp being more than double that for Tm, reaching approximately 2.5 s. The R decreases to values between 0.4 and 0.5, and a persistent overestimation of 0.7 to 1.3 s is observed in all simulations (Fig. 6c). The direction of wave propagation is best represented using the observed-based ST6 physical package. The best ST6 parameterization shows a higher correlation and lower error in Dm but also a higher bias (Fig. 6d). Specifically, Dm shows lower variability in model skills using ST4, with an RMSE of around 10°, R of approximately 0.75, and a BIAS of around −3.2° Dp statistical error metrics indicate poorer model performance in representing this variable (Fig. 6e). Overall, the ST4 parameterization exhibits similar values across all error parameters, with a BIAS greater than 1.5°, an RMSE greater than 20°, and an R <0.4. The ST6 parameterization shows, in general, better performance in representing Dp, with increasing correlation, decreasing error, and a lower bias.

A final model configuration has been selected to create a more balanced database regarding the simulation performance of all wave parameters. Three types of combinations were chosen: one that considers all the wave parameters (Hs-Tm-Tp-Dm-Dp), another that considers the height and mean parameters (Hs-Tm-Dm), and a third that considers the height and peak parameters (Hs-Tp-Dp). ST4 simulations show systematically better performance for the mean wave parameters than ST6 (Fig. 7), the peak wave parameters show the highest MPS in a ST6 parametrization (C.24), but it is closely followed by the MPS of a ST4 parametrization (C.06). Finally, the combination of all wave parameters shows that the simulation performs best is C.06. Therefore, the ST4 package with βmax =1.52; Cds =-3.0×10^{-5} and Br =9×10^{-4} has been chosen to generate the new Chilean Wave Atlas (AOC3).

3.2. Validation

This section presents a validation of the AOC3 database by

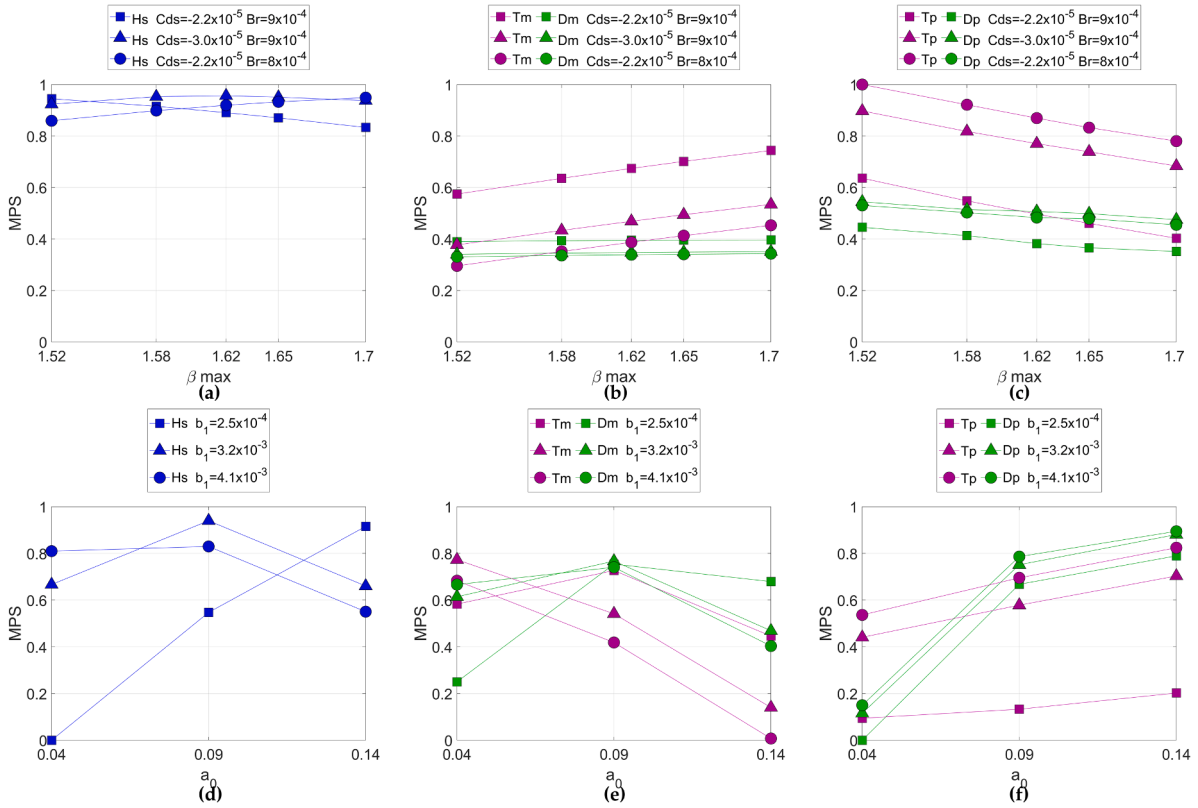

Fig. 5. Global Model Performance Score versus ST4 (up) and ST6 (down) parameters. (a-d) Significant wave height (b-e) Mean period and direction. (c-f) Peak period and direction.

comparing it with Hs satellite data, wave parameters from reanalysis, and the AOC1 data. When comparing model simulations with Hs satellite data, AOC3 performs better than AOC1, with higher correlation and lower error (Fig. 8). The AOC1 data shows a coefficient of determination $R^2 = 0.6$, BIAS $= -0.02$ m, and RMSE $= 0.83$ m, whereas AOC3 presents $R^2 = 0.9$, BIAS $= 0.06$ m, and RMSE $= 0.36$ m. This indicates an improvement in representing the variability of Hs despite a slight increase in bias.

The validation of AOC3 with other available hindcasts is presented based on wave records from a buoy off the coast of Valparaíso. The results indicate that all datasets overestimate the Hs, with BIAS values ranging from 0.1 m to 0.4 m, and the AOC3 distinguished as the hindcast with the lower BIAS (Fig. 9a). The RMSE ranged from 0.30 m to 0.40 m, and R between 0.8 and 0.9, showing the best (worst) performance in the hindcast ERA5 (CONV). The rest of the hindcasts exhibit close RMSE and R values each other. Dm highlights the best performance of ERA5 and AOC3 datasets; both hindcasts have similar RMSE and R values (Fig. 9b). However, the ERA5 (AOC3) data show a slight negative (positive) BIAS. Tp exhibits the RMSE of around 2.5 s, the BIAS ranged between 0.3 and 0.5 s, and R was between 0.45 and 0.55, with ERA5 performing best, followed closely by AOC3 data (Fig. 9c).

Finally, when comparing Hs outputs Hs of AOC1 and AOC3 with HsSAT from the along-track data detailed in section 2.3, the RMSE ranged from 0.20 m to 0.70 m, the BIAS was ± 0.80 m, and R ranged from 0.65 to 0.99, highlighting the superior performance of AOC3, followed by CONV (Fig. 10).

4. Discussion

In general, the AOC3 data effectively captures the key aspects of the wave climate in the study region. The simulation demonstrates a reasonable agreement with buoy observations, showing biases of ± 0.16 m for Hs, an underestimation of Tm lower than 0.72. *sec*, an overestimation of Tp lower than 1.4 s, and $\pm 12^{\circ}$ for wave direction. The calibration process shows that the model systematically overestimates the Tp. This overestimation results from the model's prediction of longer wave periods in the Southern Ocean, significantly influencing the wave climate in the Southeast Pacific due to the Southern Ocean swell predominates (Beyá et al., 2016; Aguirre et al., 2017). This positive bias in Southern Ocean swell is consistent with previous studies that reported overestimated wave energy along exposed coastlines of the Southern Hemisphere, such as southwestern Australia (Q. Liu et al., 2021;J. Liu et al., 2022).

Although global spectral models such as WW3 continuously perform well in representing Hs, accurately simulating wave period and direction remains challenging, particularly its peak values Tp and Dp. For example, an accurate description of the wave period also improves potential energy diagnostics for the use of wave energy converters (e.g. J. Liu et al., 2023; Mediavilla and Sepúlveda, 2016). Also, wave direction is crucial when propagating deep water spectral information toward the coast; directional variations of $\pm 10^{\circ}$ can significantly impact the wave energy entry into a semi-enclosed bay. These exemplify that based on model performance scores, the calibration process presented here is a flexible quantitative decision tool to define the most favorable configuration of wave hindcast models depending on the wave parameter and error metrics one wants to prioritize. This performance score can be used independently or in an aggregated mode, depending on the model application of interest.

The first Chilean Wave Atlas (AOC1) was described by Beyá et al. (2017). This hindcast was forced by ERA-Interim reanalysis and uses the C.01 configuration. Our calibration processes achieved the best performance using the C.06 configuration. The only difference between C.01 and C.06 is the dimensionless parameter Cds in the energy dissipation equation (Ardhuin et al., 2010). Although C.01 and C.06 show similar performance scores when considering Hs, Tm, and Dm, changing Cds to -3.0×10^{-5} significantly improves the Tp and Dp model scores when

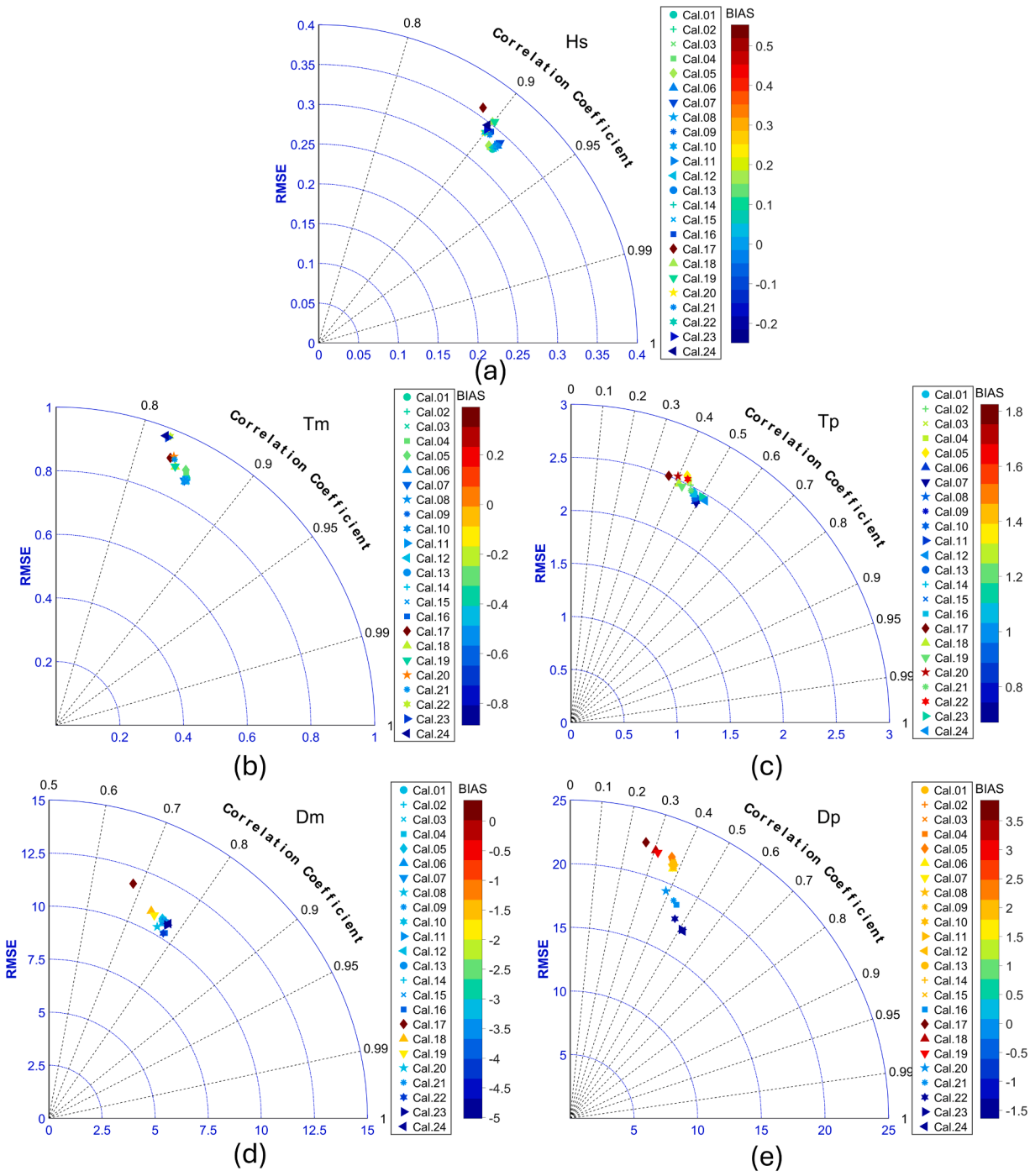

Fig. 6. Error metrics diagram using wave parameters observations from wave buoys (a) Significant wave height (b) Mean period (c) Peak period (d) Mean direction (e) Peak direction.

ERA5 data is used to force the model. This new hindcast (AOC3) resulted in improved error statistical parameters when compared with satellite Hs along the coast of Chile, with a significant increase in the coefficient of determination R^2 from 0.60 to 0.92 and a decrease in RMSE from 0,83 m to 0,36 m. In Fig. 8, AOC1 shows a spread of scatter points that diverge from the 1:1 line. This pattern is mainly produced in north and central Chile, where AOC1 performs worst. In fact, Beyá et al. (2017) introduced a blend of correction of systematic errors after the calibration process that significantly improved the performance of AOC1. It is important to note that this dispersion pattern is not observed in AOC3, making a significant improvement without applying any corrections to the simulated wave parameters.

Comparison with other hindcasts showed that AOC3 performed well on the central Chilean coast. However, using wave data from a buoy off Valparaíso, the best skills are found for the ERA5 hindcast in Hs, Tp, and Dm. A distinct characteristic of the ERA5 hindcast is that it incorporates coupled processes due to the ocean wave parameters generated from a fully coupled atmosphere-wave model (Hersbach et al., 2020). Thus, in future upgrades of the Chilean Wave Atlas, a focus will be the implementation of coupled regional models that integrate wave dynamics with other physical processes, such as atmospheric and ocean circulation. Initial efforts in coupling have been performed in Chile for a more comprehensive approach, accounting for the interactions and feedback mechanisms between waves, winds, and currents (Bahamóndez and

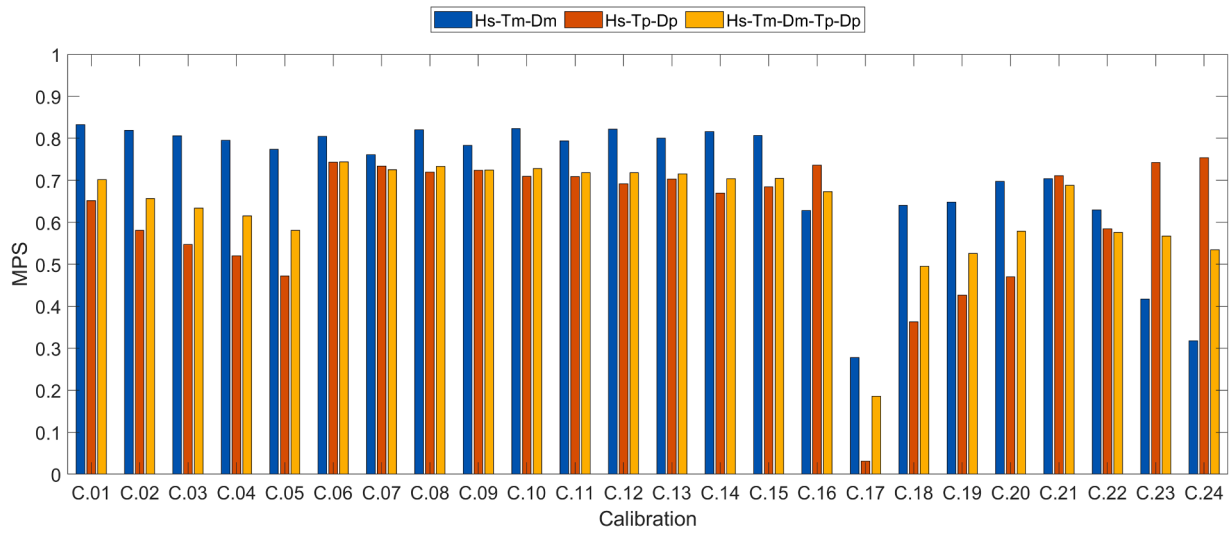

Fig. 7. Combination of model performance score (MPS) for each simulation. The blue bar represents the combined MPS for Hs, Tm, and Dm. The orange bar represents the combined MPS for Hs, Tp, and Dm. The yellow bar represents the combined MPS for all wave parameters.

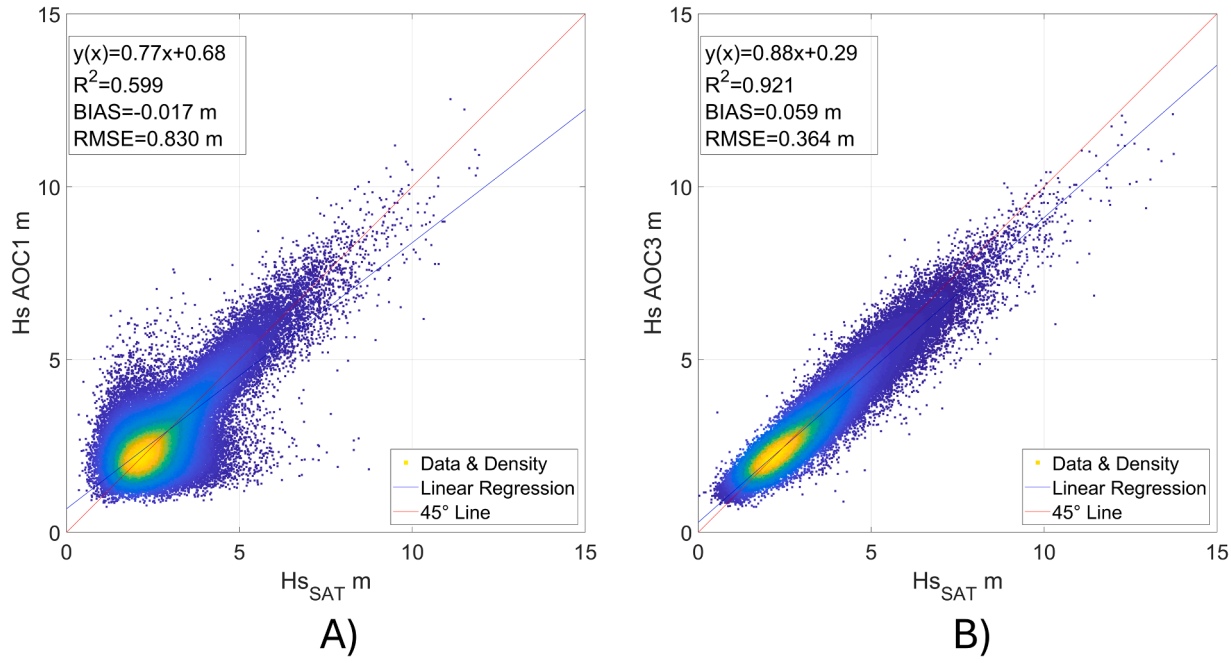

Fig. 8. Scatter plot colored by density data of HsSAT vs simulated Hs. The red line is the perfect simulation, and the blue line is the linear regression of the data for (left) AOC1 (Beyá et al.,2017) and (right) AOC3.

Aguirre, 2023). Additionally, we aim to increase the model's spatial resolution, particularly in coastal regions where wave behavior is strongly influenced by localized features such as bathymetry, shoreline configuration, and nearshore currents.

This provides a solid foundation for future research, offering insights into long-term wave patterns, trends, and extremes that would otherwise remain unknown. Additionally, a validated hindcast can serve as critical boundary conditions for more localized or high-resolution models through the nesting process, allowing researchers to zoom in on specific regions of interest with greater detail and accuracy. This approach supports more informed decision-making in coastal management, infrastructure planning, and climate impact assessments, especially in data-poor areas where wave dynamics are poorly understood. Enhancing the wave model's performance enables a deeper understanding of how waves can impact the coastal socio-ecosystems, facilitating better shoreline management and the development of territorial planning policies that better prepare communities for climate change adaptation.

5. Conclusions

This work presented a detailed calibration process for updating the Chilean Wave Atlas using the WaveWatch III model forced with ERA5 reanalysis data. We focused on the semi-empirical ST4 parameterization, conducting 15 distinct simulations and 9 simulations using the observed-based ST6 parameterization. Compared with buoy observations, all simulations performed better for wave heights than wave periods and directions. Improvement is particularly needed for simulating wave peak parameters such as Tp and Dp. Overall, the ST4 physics package demonstrated the best performance, with slight variation in

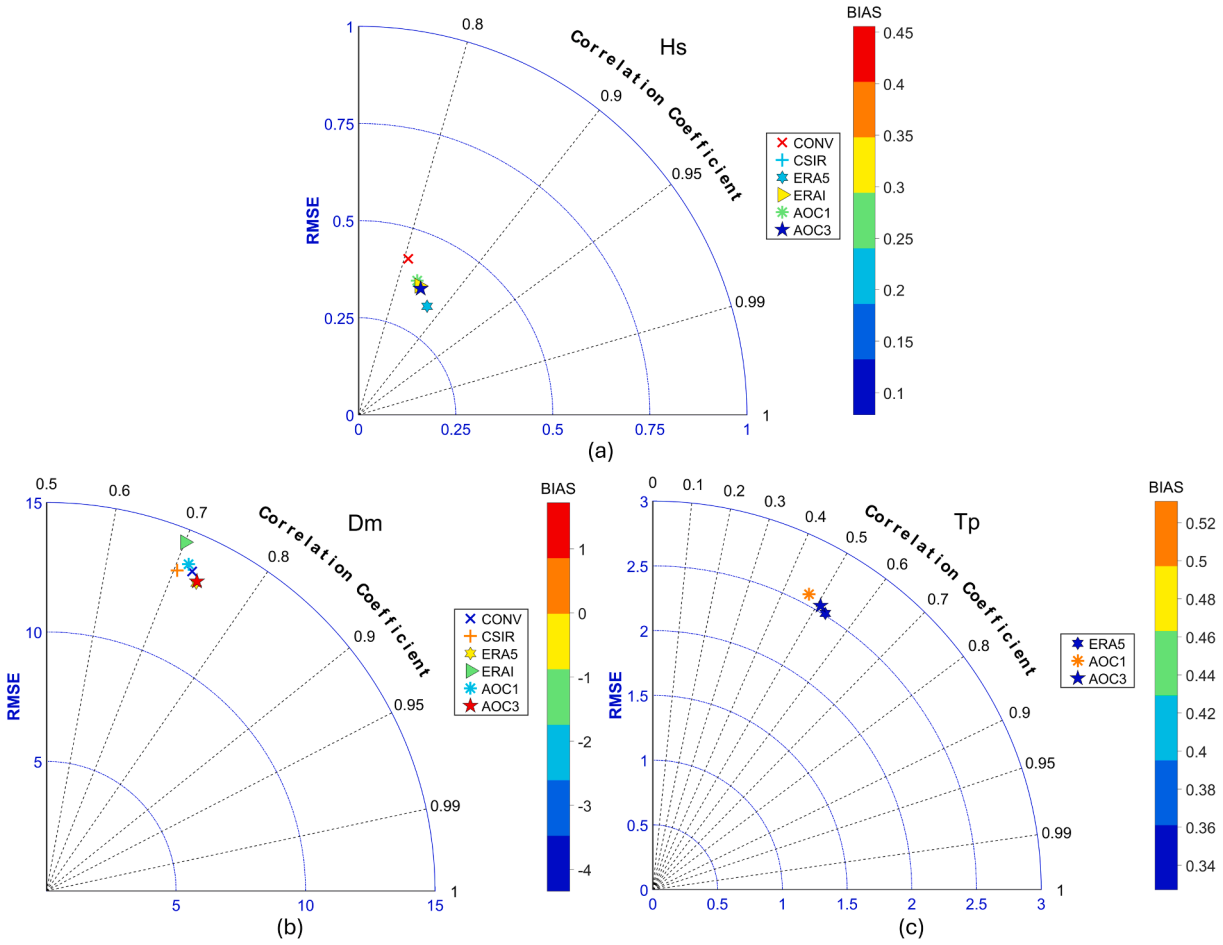

Fig. 9. Error metrics diagram using observed wave data from the Valparaíso buoy compared to CONV, CSIR, ERA5, ERAI, AOC1 and AOC3 for (a) Hs. (b) Dm. (c) Tp.

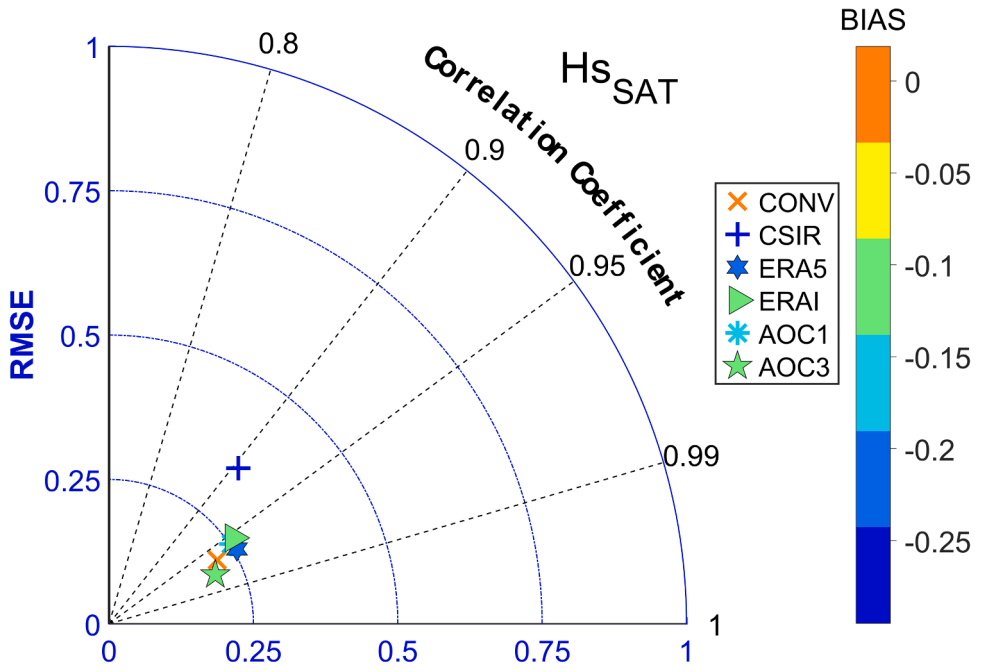

Fig. 10. Error metrics diagram using observations of Hs_{SAT} along-track data compared to Hs for CONV, CSIR, ERA5, ERAI, AOC1 and AOC3.

error metrics between different simulations, particularly for modeled Hs. However, the ST6 parameterization notably produced better results for wave direction, both Dm and Dp.

Using performance scores as a quantitative tool to define the optimal configuration of the wave model, we evaluated the 24 distinct simulations. We identified the best results for the updated Chilean Wave Atlas (AOC3) corresponding to the C.06 parameterization. Employing this configuration, a final hindcast was generated between 1979 and 2022, containing hourly fields of Hs, Tm, Tp, Dm, and Dp for the Pacific Ocean, as well as 72 directional spectra, mainly along its eastern boundary. Comparison with satellite Hs data along the Chilean coast demonstrated that this new dataset, AOC3, significantly improves the performance of AOC1 without the need for any systematic correction to the simulated Hs. Unlike other freely available hindcasts, AOC3 is specifically calibrated and validated for Chilean coasts. In fact, AOC3 presented the best model performance compared to other available hindcasts when using remotely observed wave height. However, it is also worth mentioning the good performance of the ERA5 wave parameters when compared with buoy data, possibly highlighting the importance of model-coupled processes.

The AOC1 and new AOC3 datasets are freely available at www.oleaje.uv.cl. This information is expected to be valuable for teaching, academic research, and engineers concerned with wave climate and coastal infrastructure projects in this region. Future enhancements of the Chilean Wave Atlas will focus on testing coupling tools of WW3 with other regional atmospheric and ocean models, as well as wave propagation toward nearshore coastal waters.

CRediT authorship contribution statement

Sebastian Omar Correa Araya: Writing – original draft, Visualization, Validation, Software, Methodology, Investigation, Formal analysis, Data curation, Conceptualization. **Catalina Aguirre:** Writing – review & editing, Writing – original draft, Software, Project administration, Methodology, Investigation, Funding acquisition, Conceptualization. **Diego Becerra:** Software, Investigation. **Mauricio Molina:** Project administration, Funding acquisition, Conceptualization. **Pablo Vilchez:** Visualization, Validation, Formal analysis. **Sergio Bahamóndez:** Visualization, Validation, Formal analysis.

Declaration of competing interest

The authors declare that they have no known competing financial interests or personal relationships that could have appeared to influence the work reported in this paper.

Acknowledgments

The authors thank the National Research and Development Agency, which is part of the Ministry of Science, Technology, Knowledge, and Innovation of the Government of Chile, for funding within the FONDEF IDeA I+D ID20I10404 Program framework. CA mainly thanks to the support of FONDAP 1523A0002. We also acknowledge Gillian Ord for her support in writing and grammar details. Powered@NLHPC: This research was partially supported by the supercomputing infrastructure of the NLHPC (ECM-02).

Supplementary materials

Supplementary material associated with this article can be found, in the online version, at doi:10.1016/j.ocemod.2024.102456.

Data availability

Data will be made available on request.

References

Aguirre, C., Rutllant, J.A., Falvey, M., 2017. Wind waves climatology of the Southeast Pacific Ocean. Int. J. Climatol. 37 (12). https://doi.org/10.1002/joc.5084.

Amarouche, K., Akpınar, A., Bachari, N.E.I., Çakmak, R.E., Houma, F., 2019. Evaluation of a high-resolution wave hindcast model SWAN for the West Mediterranean basin. Appl. Ocean Res. 84. https://doi.org/10.1016/j.apor.2019.01.014.

Ardhuin, F., Rogers, E., Babanin, A.V., Filipot, J.F., Magne, R., Roland, A., van der Westhuysen, A., Queffeulou, P., Lefevre, J.M., Aouf, L., Collard, F., 2010. Semiempirical dissipation source functions for ocean waves. Part I: Definition, calibration, and validation. JournalofPhysicalOceanography 40 (9). https://doi.org/10.1175/2010JPO4324.1.

Babanin, A.V., 2017. Wave Breaking and Dissipation. Encycloped. Maritime Offshore Eng. https://doi.org/10.1002/9781118476406.emoe082.

Badriana, M.R., Lee, H.S., 2020. Evaluation and bias correction of marine surface winds in the western north pacific from CMIP5 and CMIP6 GCMS for wave climate modelling. Coast. Eng. Proc. 36v. https://doi.org/10.9753/icce.v36v.waves.35.

Bahamóndez, S., Aguirre, C., 2023. Sistema de simulación numérica para la costa de Chile central mediante el acoplamiento de modelos numéricos. Obras y Proyectos. https://doi.org/10.21703/0718-281320233302.

Beyá, J., Álvarez, M., Gallardo, A., Hidalgo, H., Aguirre, C., Valdivia, J., Parra, C., Méndez, L., Contreras, C., Winckler, P., Molina, M., 2016. Atlas De Atlas de Oleaje de Chile. Primera edición. Economia.

Beyá, J., Álvarez, M., Gallardo, A., Hidalgo, H., Winckler, P., 2017. Generation and validation of the Chilean Wave Atlas database. Ocean. Model. (Oxf) 116. https://doi.org/10.1016/j.ocemod.2017.06.004.

Cao, D., Tolman, H.L., Chen, H.S., Chawla, A., Gerald, V.M., 2007. Performance of the ocean wave ensemble forecast system at NCEP. In: 10th International Workshop on Wave Hindcasting and Forecasting & Coastal Hazards Symposium, 279.

Cavaleri, L., Fox-Kemper, B., Hemer, M., 2012. Wind waves in the coupled climate system. Bull. Am. Meteorol. Soc. 93 (11). https://doi.org/10.1175/BAMS-D-11-00170.1.

Arun, Chawla, Tolman Hendrik, L, 2007. Automated grid generation for WAVEWATCH III. In: NOAA National Centers for Environmental Prediction.

Dee, D.P., Uppala, S.M., Simmons, A.J., Berrisford, P., Poli, P., Kobayashi, S., Andrae, U., Balmaseda, M.A., Balsamo, G., Bauer, P., Bechtold, P., Beljaars, A.C.M., van de Berg, L., Bidlot, J., Bormann, N., Delsol, C., Dragani, R., Fuentes, M., Geer, A.J., Vitart, F., 2011. The ERA-Interim reanalysis: Configuration and performance of the data assimilation system. Q. J. R. Meteorol. Soc. 137 (656). https://doi.org/10.1002/qj.828.

Dodet, G., Piolle, J.F., Quilfen, Y., Abdalla, S., Accensi, M., Ardhuin, F., Ash, E., Bidlot, J. R., Gommenginger, C., Marechal, G., Passaro, M., Quartly, G., Stopa, J., Timmermans, B., Young, I., Cipollini, P., Donlon, C., 2020. The Sea State CCI dataset v1: Towards a sea state climate data record based on satellite observations. Earth. Syst. Sci. Data 12 (3). https://doi.org/10.5194/essd-12-1929-2020.

Durrant, T., Hemer, M., Trenham, C., Greenslade, D., 2013. CAWCR wave hindcast extension Jan 2011 - May 2013. v5. CSIRO. Service Collection.

Fan, Y., Lin, S.J., Held, I.M., Yu, Z., Tolman, H.L., 2012. Global ocean surface wave simulation using a coupled atmosphere-wave model. JournalofClimate (18), 25. https://doi.org/10.1175/JCLI-D-11-00621.1.

Goda, Y., 2010. Random seas and design of maritime structures. In: Random Seas And Design Of Maritime Structures, 3rd Edition. https://doi.org/10.1142/7425. 3rd Edition.

Hemer, M.A., Katzfey, J., Trenham, C.E., 2013. Global dynamical projections of surface ocean wave climate for a future high greenhouse gas emission scenario. Ocean. Model. (Oxf) 70. https://doi.org/10.1016/j.ocemod.2012.09.008.

Hersbach, H., Bell, B., Berrisford, P., Hirahara, S., Horányi, A., Muñoz-Sabater, J., Nicolas, J., Peubey, C., Radu, R., Schepers, D., Simmons, A., Soci, C., Abdalla, S., Abellan, X., Balsamo, G., Bechtold, P., Biavati, G., Bidlot, J., Bonavita, M., Thépaut, J.N., 2020. The ERA5 global reanalysis. Q. J. R. Meteorol. Soc. 146 (730). https://doi.org/10.1002/qj.3803.

Komar, P.D., 1998. Beach Processes and Sedimentation, 2. Prentice-Hall.

Kousal, J., Voermans, J.J., Liu, Q., Heil, P., Babanin, A.V., 2022. A Two-Part Model for Wave-Sea Ice Interaction: Attenuation and Break-Up. Journal of Geophysical Research: Oceans 127 (5). https://doi.org/10.1029/2022JC018571.

Liu, J., Meucci, A., Liu, Q., Babanin, A.V., Ierodiaconou, D., Xu, X., Young, I.R., 2023. A high-resolution wave energy assessment of south-east Australia based on a 40-year hindcast. RenewableEnergy 215. https://doi.org/10.1016/j.renene.2023.118943.

Liu, J., Meucci, A., Liu, Q., Babanin, A.V., Ierodiaconou, D., Young, I.R., 2022. The wave climate of Bass Strait and South-East Australia. Ocean. Model. (Oxf) 172. https://doi.org/10.1016/j.ocemod.2022.101980.

Liu, Q., Babanin, A.V., Rogers, W.E., Zieger, S., Young, I.R., Bidlot, J.-R., Durrant, T., Ewans, K., Guan, C., Kirezci, C., Lemos, G., MacHutchon, K., Moon, I.-J., Rapizo, H., Ribal, A., Semedo, A., Wang, J., 2021. Global Wave Hindcasts Using the Observation-Based Source Terms: Description and Validation. J. Adv. Model. Earth. Syst. 13 (8), e2021MS002493. https://doi.org/10.1029/2021MS002493.

Liu, Z., & Frigaard, P. (1999). *Generation and Analysis of Random Waves (Part 2)*. 1.

Mediavilla, D.G., Sepúlveda, H.H., 2016. Nearshore assessment of wave energy resources in central Chile (2009-2010). RenewableEnergy 90. https://doi.org/10.1016/j.renene.2015.12.066.

NOAA National Geophysical Data Center, 2006. 2-minute Gridded Global Relief Data (ETOPO2) v2. NOAA National Centers for Environmental Information. https://doi.org/10.7289/V5J1012Q.

Pavlova, A., Myslenkov, S., Arkhipkin, V., Surkova, G., 2022. Storm Surges and Extreme Wind Waves in the Caspian Sea in the Present and Future Climate. Civil Engineering Journal (Iran) 8 (11). https://doi.org/10.28991/CEJ-2022-08-11-01.

Ramon, J., Lledó, L., Torralba, V., Soret, A., Doblas-Reyes, F.J., 2019. What global reanalysis best represents near-surface winds? Q. J. R. Meteorol. Soc. 145 (724). https://doi.org/10.1002/qj.3616.

Rogers, W., Babanin, A.v., Wang, D.W., 2012. Observation-consistent input and whitecapping dissipation in a model for wind-generated surface waves: Description and simple calculations. J. Atmos. Ocean. Technol. 29 (9). https://doi.org/10.1175/JTECH-D-11-00092.1.

Servicio Hidrográfico y Oceanográfico de la Armada de Chile, 2009. Pub. 3201 Instrucciones oceanográficas Nº1. Servicio Hidrográfico y Oceanográfico de la Armada de Chile. https://shoabucket.s3.amazonaws.com/shoa.cl/documentos/publicaciones/ins_oceonograficas/3201.pdf.

Shimura, T., Mori, N., 2019. High-resolution wave climate hindcast around Japan and its spectral representation. Coast. Eng. 151. https://doi.org/10.1016/j.coastaleng.2019.04.013.

Silva, R., 2005. *Análisis y Descripción Estadística Del Oleaje* (Vol. 1). Instituto de Ingeniería. UNAM.

Smith, G.A., Hemer, M., Greenslade, D., Trenham, C., Zieger, S., Durrant, T., 2021. Global wave hindcast with Australian and Pacific Island Focus: From past to present. Geosci. Data J. 8 (1). https://doi.org/10.1002/gdj3.104.

Soran, M.B., Amarouche, K., Akpınar, A., 2022. Spatial calibration of WAVEWATCH III model against satellite observations using different input and dissipation parameterizations in the Black Sea. Ocean Engineering 257. https://doi.org/10.1016/j.oceaneng.2022.111627.

The WAVEWATCH III Development Group, 2019. User manual and system documentation of WAVEWATCH III version 6.07. In: Tech. Note 333, NOAA /NWS / NCEP / MMAB, College Park,MD,USA,465 Pp, 333.

Wessel, P., Smith, W.H.F., 1996. A global, self-consistent, hierarchical, high-resolution shoreline database. Journal of Geophysical Research: Solid Earth 101 (4). https://doi.org/10.1029/96jb00104.

Wessel, P., Smith, W.H.F., 2015. Global Self-consistent, Hierarchical, High-resolution Geography Database (GSHHG). NOAA National Geophysical Data Center.

Zieger, S., Babanin, A.v., Erick Rogers, W., Young, I.R, 2015. Observation-based source terms in the third-generation wave model WAVEWATCH. Ocean. Model. (Oxf) 96. https://doi.org/10.1016/j.ocemod.2015.07.014.